HHS Public Access

Author manuscript

Crit Rev Biomed Eng. Author manuscript; available in PMC 2016 July 11.

Published in final edited form as:

Crit Rev Biomed Eng. 2011 ; 39(1): 63–77.

Wireless Microstimulators for Neural Prosthetics

Mesut Sahin[1,*] and **Victor Pikov**[2]

[1]Biomedical Engineering Department, New Jersey Institute of Technology, Newark, NJ

[2]Neural Engineering Program, Huntington Medical Research Institutes, Pasadena, CA

Abstract

One of the roadblocks in the field of neural prosthetics is the lack of microelectronic devices for neural stimulation that can last a lifetime in the central nervous system. Wireless multi-electrode arrays are being developed to improve the longevity of implants by eliminating the wire interconnects as well as the chronic tissue reactions due to the tethering forces generated by these wires. An area of research that has not been sufficiently investigated is a simple single-channel passive microstimulator that can collect the stimulus energy that is transmitted wirelessly through the tissue and immediately convert it into the stimulus pulse. For example, many neural prosthetic approaches to intraspinal microstimulation require only a few channels of stimulation. Wired spinal cord implants are not practical for human subjects because of the extensive flexions and rotations that the spinal cord experiences. Thus, intraspinal microstimulation may be a pioneering application that can benefit from submillimetersize floating stimulators. Possible means of energizing such a floating microstimulator, such as optical, acoustic, and electromagnetic waves, are discussed.

Keywords

neuroprosthetics; neurostimulation; microstimulation; floating stimulator; infrared tissue penetration; radiofrequency telemetry; ultrasound power transfer; energy harvesting

I. INTRODUCTION

Neural stimulation with microscale electrodes is constantly finding new applications in the central nervous system (CNS). As new neuroprosthetic and neuromodulation applications are being tested in animal models, the field is facing a number of challenges in its transition to the clinic. A chronically implantable microelectrode array that can last a lifetime is a goal yet to be achieved. Device failures commonly occur due to the breakage of wire interconnects[1] and chronic tissue response due to micromotion of electrodes. [2–4] Recently, durable and flexible wire assemblies have been shown to function for several years in the cortex.[5,6] Such flexible interconnects may provide sufficient longevity for cortical implants, but the tethering problem remains a challenging issue for neuroprosthetics in more mobile

[*]Address all correspondence to Mesut Sahin, PhD, Biomedical Engineering Department, New Jersey Institute of Technology, Newark, NJ 07102; sahin@njit.edu.

parts of the CNS. The interconnect longevity is, for instance, rarely more than one year in the feline spinal cord.[7]

In humans, the axial mobility of a brainstem is 0.8–1.6 mm and the rotational mobility of the cerebellum is 2.7–4.3° during voluntary movements over the normal range of head/neck flexion.[8] Under low-severity impacts, the brain can undergo significant translational (4–5 mm) and rotational (4–5°) displacement.[9] The spinal cord can experience even greater translational and rotational displacements. The log-roll rehabilitation technique, developed for patients with traumatic spinal cord injury, generates 7.9° and 21.2° of axial rotation in the cervical and lumbar cord, respectively, as tested in cadavers.[10] Thus, elimination of wire connections between the implant and the external electronics is essential to achieve adequate longevity for chronically implantable electrode in the spinal cord and possibly in other parts of the CNS. Power and data telemetry approaches developed for micro-electrode arrays have been extensively covered elsewhere both for recording[11,12] and stimulation applications,[13,14] and thus will not be addressed in this review. Instead, we will discuss the feasibility of a single-channel wireless microstimulator that receives and instantly converts the energy to a stimulus current without using any active electronics on the implant. A number of new applications, especially in the spinal cord, can open up if such microstimulators can be realized in submillimeter sizes. These microscale floating stimulators can be implanted in the most mobile parts of the CNS with minimal insult to the surrounding neural tissue to be used for long-term microstimulation.

II. PASSIVE VS. ACTIVE STIMULATORS

Neural stimulation often employs a train of rectangular current- or voltage-regulated pulses that are delivered at a specific frequency and temporal pattern. In addition, recent studies evaluated the potential benefits of nonrectangular pulse wave-forms. [15,16] When the wire connections are eliminated, two choices appear for the placement of the control electronics for stimulus pattern generation and channel selection: placement on the electrode assembly or on the external controller. In the former case, complex digital and analog circuits need to be incorporated into the limited space on the implanted device in order to store the stimulus parameters and deliver the stimuli in a specific pattern. The latter case, on the other hand, opens up the possibility of eliminating the active electronics on the implant altogether since the energy transfer to the device can be achieved on a pulse-by-pulse basis. Elimination of active electronics reduces the implant to a passive device that does not require continuous power through wireless connection or from an internal battery. This approach, which is the subject of this article, has not been explored sufficiently to date.

If the implanted stimulator consists of a simple transducer and perhaps a few electronic components that instantly convert the energy into an electrical current for neural stimulation, we can classify these devices as passive wireless stimulators (Fig. 1) as opposed to active devices that contain complex electronics to store the pulse parameters and generate the stimulus pattern at a later time. The choices for energy transfer to a passive device, including the electromagnetic, optical, and acoustic methods, will be discussed in the following section. The fact that no active electronics are utilized in the conversion of the stimulus energy into electrical pulse patterns imposes additional constraints on the design of the

microstimulator. The added engineering efforts required to realize a passive floating stimulator at submillimeter scale may still be worthwhile. A tether-free microstimulator may overcome the roadblocks faced by a number of wired neural prosthetic devices on their path to the clinic. Eliminating the wire interconnects can potentially reduce the tissue response that is mostly generated by the tethering forces of the wires, eliminate the problem of wire breakage and device failures due to electronics, and increase the functional device life, all of which are essential prerequisites for long-term implants. Next, we will discuss the feasibility and some design criteria of such microstimulators.

III. ENERGY TRANSFER TO A MICROSTIMULATOR

A. Radio-Frequency Power Telemetry

Power telemetry for microstimulation devices is commonly provided by radio frequency (RF) due to low absorption of these electromagnetic waves in tissue.[17] The RF power transfer is mediated by inductive coupling between the coaxially positioned transmitting and receiving antennas. Choice of the frequency of operation in the RF band is based on a trade-off between the antenna size and the depth of RF penetration, both of which are very important for neural implants.[17,18] The antenna size is often a limiting factor for the overall size of the implant and can take up a large portion of the implant volume. [19] Reduction in the implant dimensions can allow more accurate targeting in the nervous system, as well as reduced implantation trauma and chronic immune response. It is important to note that the size of the implanted antenna in neural implants can be reduced 10- to 20-fold relative to the air-based RF transmission due to considerable shortening of the RF waves in the human body. The wave shortening is a result of wave attenuation in the tissue and is proportional to a square root of relative tissue permittivity, tissue conductivity, and RF frequency.[20] The water with dissolved ions is a main source of increased tissue permittivity and ionic conductivity,[21] which explains why at 2.45 GHz (wavelength = 12 cm), the penetration depth in fat is 11 cm, while in water-rich tissues, such as brain, muscle, or skin, it is 2 cm.[22] The frequency range of 3–30 GHz (1–10 cm) may provide a good compromise between the size of the antenna and tissue penetration, both of which are on the order of a few mm in this frequency range.[17,23]

The receiving antenna geometry, either coiled or straight wire, is determined by the dimensions of the microstimulator. The coil-based antenna can be made more compact than a straight antenna in terms of the overall implant size, for instance, allowing a 480-kHz-operated microstimulation device, the BION, to be implanted though a 12-gauge (2.8 mm) needle.[24] The straight wire antenna, in contrast, can reduce the cross-sectional area of the device at the expense of its axial dimension, which can be beneficial for a less-traumatic injection through a smaller-gauge needle. In addition to the wire-based antennas, thin films have been used for harvesting the RF power either as thin-film inductive coils[25] or as thin-film linear antenna arrays.[26] Such thin-film antennas are particularly useful for microstimulators to be implanted on the surface of neural tissue (e.g., epidurally or subdurally) to take advantage of their flexible planar geometry.

The power transfer efficiency depends on the dimensions and geometry of the transmitting and receiving antennas as well as the distance between the antennas.[27] At a high antenna

coupling factor of 15%, the power transfer efficiency can reach 70%; but when a coupling factor drops to a low level of 2%, the maximal efficiency can reach only 10%.[27] Because of RF energy absorption by the human body, tissue heating becomes a limiting factor in the power transmission to the implanted microstimulator. It is estimated that absorption of 10 mW of power at 1–5.8 GHz by the human head produces only a negligible temperature rise of 0.01–0.02°C.[28] Basal metabolic rate, ~1 W/kg in an adult person,[29] is commonly used as the safe limit for RF absorption in the tissue in order to avoid an uncomfortable warm sensation or heat-induced trauma in the body.

The conversion of the RF energy into a direct current (DC) at the implant can be done through a p-n junction based transistor (e.g., FET) or a metal-semiconductor junction based Schottky transistor or diode.[30] In the GHz range, the Schottky transistor is a preferred transistor type as it can operate at much higher frequencies (up to 100 GHz) compared to FET (< 1 GHz) due to its higher electron mobility and smaller capacitance.[30] Another advantage of the Schottky transistor/diode is its straightforward integration with the linear antenna for a compact RF-to-DC conversion unit that can be easily multiplied for an array design.[26] One of the commercial neurostimulation devices, the BION®, uses the Schottky diode for RF-to- DC conversion followed by an electrolytic capacitor, thus allowing the stimulation charge to build up between the pulses and be able to inject currents up to 100 times the instantaneous DC current provided by the inductive link.[19] The first generation of this cylindrical device had a diameter of 2 mm and a length of 16 mm. The second-generation device had an increased voltage compliance of 18 V and current injection capabilities up to 30 mA.[24] A more recent version includes a rechargeable battery and sensors[31] with dimensions of 27 mm length and 3.3 mm diameter. The BION® device has been clinically tested for several applications in the peripheral nervous system, such as shoulder subluxation in post-stroke patients, pressure ulcer prevention, obstructive sleep apnea, overactive bladder, and migraine therapy;[32] however, it is not suitable for the CNS applications due to its large size. Another single-channel microstimulator with RF telemetry was reported to consume 45–55 mW and measure 2 × 2 ×10 mm in size[33] and tested for reanimation of paralyzed laryngeal muscles.[34]

B. Pulsed Ultrasound (PUS) Power Telemetry

The PUS approach has been successfully tested for power telemetry to a cardiac muscle stimulator[35,36] but is yet to be investigated in neuroprosthetic devices, with an exception of a brief study[37] where the stimulator consisted of a lead zirconate titanate (PZT) transducer and a rectifier diode. A frog sciatic nerve was stimulated with this device using 2.25 MHz of ultrasound signal at a peak power of 2.5 W/cm^2. The reported size of this prototype device was about 11 mm in length and no electronics were contained in the stimulator except for a single rectifier diode.

In general, the PUS generator is composed of piezoelectric ceramic material, has an aperture diameter of several cm, and operates at frequencies of several kHz.[35] In the microstimulator, the vibro-electric conversion can be done using a 2D MEMS resonator generating AC that is converted to DC with a Schottky diode.[38] At a depth of 10 cm into the tissue, the efficiency of vibro-electric energy conversion is estimated to be ~0.07%.[36] At the same depth of 10

cm, the PUS applied with the peak acoustic intensity of 71 W/cm^2 and average intensity of 178 mW/cm^2 produces no evidence of necrosis or hemorrhage in the tissue.[35] The FDA guidance limits the prolonged PUS body exposure to the peak acoustic intensity of 190 W/cm^2 and average intensity of 430 mW/cm^2.[39,40] For applications in the brain and spinal cord, additional safety concerns in PUS exposure relate to opening the blood-brain barrier when applied at a pressure of 670 kPa[41] and direct induction of brain activity when applied at the peak acoustic intensity of 2.9 W/cm^2.[42] Another possible challenge for applying PUS for power telemetry involves its susceptibility to interference from environmental acoustic noise sources, such as those generated by turbulence during air flight or by driving on rough roads.[43]

C. Near-Infrared Power Telemetry

Near-infrared (NIR) power telemetry has received less attention due to its limited penetration through the bone and skin tissue. It has been used in only a few specific neural stimulation paradigms: (1) light delivery through an optical fiber located in the vicinity of a microstimulator; (2) light delivery through an optically transparent tissue, e.g., the eye, for retinal stimulation; and (3) transcutaneous light delivery for a subcutaneous peripheral nerve microstimulator. NIR light can power a microstimulator through a photovoltaic energy conversion using one or more NIR-sensitive photodiodes, commonly fabricated from silicon,[44–47] or GaAs/AlGaAs semiconductors.[48] The efficiency of photovoltaic energy conversion in the silicon photodiode placed subretinally was estimated to be ~0.3 A/W for NIR light at 780–810 nm.[46] The photodiodes based on nanoscale photo-ferroelectric thin films have also been proposed for power telemetry.[49] Due to the poor DC conduction of thin-film ferroelectrics,[50] they are capable of delivering a considerably higher photovoltage than a semiconductor photodiode, which is limited in its charge injection by the band gap of the p-n junction.[51] However, the conversion efficiency of today's ferroelectric materials is too small to be an option for floating microstimulators.

An optical fiber can be used for NIR power telemetry, especially when it is already in place (e.g., intrathecally or transcranially) for another purpose such as optogenetic neural stimulation[52] or measurement of chemical activity.[53] When the optical fiber and the photodiode(s) are properly coupled, the efficiency of photovoltaic energy conversion can reach 50% or higher.[48] For long-term implants, the drawback of such an approach would be a permanent tether between the neural tissue and the skull or skin created by the fiber, which is a potential source of inflammation, infection, and device failure. However, the device longevity can be improved significantly with this method because the wire connections are replaced by more durable optical fibers.

NIR light has been applied for power telemetry in retinal prostheses, in which the array of photodiodes is placed in the epiretinal or subretinal space.[46,47,54] The quantum efficiency in photodiodes is about thousand times lower than in retinal photoreceptors, [47] raising the concern that intense eye irradiation for photodiode power telemetry can be phototoxic to remaining retinal photoreceptors. Therefore, NIR is preferred to visible light, even though the aqueous medium and the lenses of the eye are transparent to both frequency bands. The cornea and lens are largely transparent to NIR light at 800–850 nm, and the main source of

heating is likely to be the photodiode array itself. In the in vitro tests, a long-term exposure of the 3-mm photodiode array in water to NIR at the incident power density of 110 mW/cm^2 heats the array by 1ºC.[46] Such an amount of heating approaches the safe physiological limit, but the reported temperature rise does not take into account an additional retinal capacity for absorbing the applied heat through its transperfusion with choroidal blood.[55]

NIR power telemetry was also applied transcutaneously for stimulation of peripheral nerves, although the efficiency of photovoltaic energy conversion is much lower relative to direct fiber coupling or retinal illumination due to a strong absorption and scattering of NIR light by the skin tissue. Human skin has a combined thickness of epidermal and dermal layers in most places of ~2.5 mm and has a transmittance of ~20% at 850 nm.[56] Another challenge for transcutaneous NIR power telemetry is the thermal heating of the skin, which limits the long-term irradiation of NIR light (900 nm) to the incident power density of 500 mW/cm^2, as calculated from Table 7 in Ref. 57. To maintain the intensity within the safe limits, NIR light emitted by a narrow-spot laser can be expanded (e.g., by a semispherical lens) before irradiating the skin.[44] Alternatively, NIR light can be delivered through a two-dimensional grid of low-power LEDs that are placed against the skin surface.[45]

IV. FLOATING LIGHT-ACTIVATED MICROELECTRICAL (FLAME) STIMULATOR

In this section, we will describe the design of a single-channel passive floating micro-stimulation device (Fig. 2) powered by a beam of NIR light. A microdevice that can collect the optical energy inside the tissue and then convert it into electrical current can provide neural stimulation[58–60] at much lower levels of light exposure than a direct optical stimulation technique. The simplest electro- optical device with maximum efficiency is a silicon photodiode with a large intrinsic layer to collect all the charge carriers, i.e., a P-I-N photodiode.

The critical question that needs to be addressed for the feasibility of an optical micro-electrical stimulator is whether a sufficient number of photons can be transmitted to a microstimulator implanted at some depth below the dura and be able to generate the current needed without causing excessive heating at the brain surface. The answer to this question along with a number of other parameters will determine the minimum device size that can activate the targeted neurons. The challenge is to have an optimized device design that can collect a sufficient number of photons to produce the specified current while keeping the device size small enough for the targeted implant site. Optimization of FLAME stimulators using computer simulations has been reported elsewhere.[60] Here we will discuss some critical design issues, such as NIR penetration into tissue, heating effect, and the choice of fabrication materials.

A. Heating Effect of Light Exposure

NIR wavelengths have long been recognized for their ease of penetration into living tissue compared to visible light.[61] For FLAME device optimization, the safe exposure limit of the NIR light incident on the neural tissue, e.g., the cerebral cortex or spinal cord, needs to be

determined first. Although the NIR laser beam is to be applied only as short pulses with a very low duty cycle (<4%) in most neural prosthetic applications, the heat may accumulate over time in the tissue before it can be dissipated by blood circulation. Monte Carlo simulations become useful to compute the trajectory of a photon in a medium with known absorption, scattering, and anisotropy coefficients. One can calculate the probabilistic distribution of light density in the medium by simulating the trajectory of a large number of photons. Figures 3A and 3C show the photon densities (fluence) in human white and gray matters for a circular, flat-profile laser beam aimed from above. Interestingly, the maximum photon density occurs slightly below the surface due to scattering and reflection. Photons beneath the surface have a higher chance of escaping into the top medium (air) than those that make it into deeper layers of the tissue.

All photons captured inside the tissue are absorbed eventually and converted to heat. The temperature elevation profile due to photon absorption can be computed with a finite element software for this inhomogeneous yet radially symmetrical geometry (Figs. 3B and 3D). One can then retro-spectively determine the maximum exposure limit on the surface that causes a set value of temperature increase inside the tissue. The simulations in Fig. 3 suggest that for a 0.5ºC temperature elevation (where changes in neuronal excitability start to be evident[62]), the maximum laser power is 325 mW/ cm^2 and 250 mW/cm^2 for the gray and white matters, respectively.[60]

B. NIR Penetration Depth

Next, we calculate the photon density in human gray and white matters as a function of laser beam diameter. The results in Fig. 4 indicate that the penetration depth increases with laser beam radius (while the beam intensity per unit area is kept constant) and plateaus at around 10 mm and 4 mm of beam radius for the gray and white matters, respectively. These curves suggest that increasing the beam radius beyond a certain value will not increase the photon density in deep locations of the tissue. The cost for larger beam sizes is that a larger volume of the tissue is irradiated by the photons and the temperature of a wider region is perturbed. Thus, one has to select the beam radius considering the trade-off between the photon densities needed for a specific application and the volume of tissue that will be exposed to light.

C. Materials for FLAME Stimulators

In semiconductor photodiodes, electron-hole pairs are produced everywhere photons are absorbed. The absorption coefficient strongly depends on the wavelength. Gallium arsenide (GaAs) is a direct band-gap material that has a high absorption coefficient in the visible spectrum (~400–700 nm) as well as extending up to 900 nm in the NIR range.[63] Silicon detectors are also appropriate for the visible and NIR spectral range (<1000 nm). The optical absorption coefficient of silicon, however, is one to two orders of magnitude lower than that of the direct band-band transition semiconductors such as GaAs at the NIR wavelengths. This requires a much thicker intrinsic layer (>10 m) for silicon detectors to collect a maximum number of photons, which may render the fabrication process expensive. Nevertheless, it is always worthwhile to consider silicon as a potential photodiode material because it is a mature and widely used technology.

GaAs is an attractive material for the fabrication of various electronic and micro-electromechanical (MEMS) devices. However, GaAs can release toxic materials such as As and AsO*x* that cause cell death. It was shown that GaAs surfaces can be coated with various biocompatible materials to prevent the release of toxic substances.[64] A potential coating material is Parylene C (poly-paraxylylene), which has been widely used as a structural material for bioMEMS systems, and as a coating material in electronic circuits and implantable electrodes.[65] Parylene C has several desirable properties, such as biocompatibility, chemical inertness, high flexibility, and reliable hermetic sealing of the electronic implantable systems.[66] For this application the coating material over the active area must be transparent to allow the passage of photons. Parylene C has an 80% transmittance at NIR wavelengths.[65] Xu Chao *et al.* showed that the transmittance can be improved to above 90% by depositing porous silica on Parylene C films.[67]

V. OPTIMIZATION OF A GENERIC FLOATING MICROSTIMULATOR A. Heating Effect

Although similar factors play a role in maximizing the efficiency of active devices, these criteria become more stringent with passive devices. First, the stimulus energy needs to be transferred in much more intense packets to a passive, wirelessly powered device only at times of stimulation because the pulse energy may not be stored by the implanted device. This heightens the instantaneous power dissipation, hence the heating effect in the neural tissue, regardless of the physical principle used for the energy transfer. The energy dissipation within the tissue dictates limitations on the maximum power injected at each pulse, and the minimum device size needed to collect sufficient energy for each pulse. The physical principle behind the energy transfer from the external electronics (not necessarily extracorporeal, but just outside the CNS) to the implanted microstimulator determines the energy loss across the tissue, as well as the transducer type to be used for collection of energy.

B. Bipolar vs. Monopolar

The second important factor to be considered for efficiency in a floating microstimulator is the bipolar charge delivery into tissue. That is, the contact for the return current has to be placed on the same device and therefore the separation between the anode and cathode cannot be longer than the device length. This in turn can limit the spatial extent of activation or else demand higher currents to activate a similar volume of neural tissue relative to that of a monopolar electrode. Near the bipolar electrodes, the voltage in medium is slightly less compared to the monopolar electrode, but the discrepancy increases quickly with decreasing separation between the two poles.[68] The simulations shown in Fig. 5 demonstrate this contrast between monopolar and bipolar electrodes using the activation function (AF) as a measure.[69] The peak values of AF reache farther to the right in case of the monopolar electrode. If the stimulus amplitude is varied, it can be estimated from the figure that volume of activation is smaller with bipolar electrodes, particularly at large stimulus amplitudes. But the difference becomes less for small volumes of activation as the stimulus amplitude is decreased.

The third issue, which is common to both active and passive electrodes but is a more stringent criterion in the design of passive stimulators, is the power loss across the electrode contacts. The material chosen for the contacts can directly affect the overall efficiency, hence the device size.

C. Selection of Contact Material

Once the stimulus energy is collected by the implanted device, it needs to be transferred to the targeted neural tissue in an efficient way. Low efficiency in either energy collection or energy transfer would require an increase in the device size itself regardless of the physical principle used for wireless power transfer. Charge injection capacity (CIC) of the contact material as well as the contacts' shape, size, and location play a major role in efficient transfer of stimulus pulse to the surrounding neural tissue. Injection of high currents through microscale contacts imposes challenges for the electrode-electrolyte interface. Whether the current is injected through faradaic or capacitive mechanisms, the voltage across the interface is limited by the water window. Several materials have been investigated for their high CIC. The iridium oxide (IrOx) contacts obtained either by activation of iridium or a sputtering process can achieve very large CIC values as measured under biphasic pulsing.[70] (The CIC of an IrOx electrode might be somewhat less with chronic implants in live tissue.[71]) The very high CIC values reported for the IrOx electrodes are achieved by anodically biasing the electrode, which necessitates a built-in active circuitry on the device. Therefore, other materials that can provide comparable CIC values at the open-circuit voltage of the interface may be a better choice for a passive floating microstimulator. If the mechanism for charge injection is faradaic, then these chemical reactions should be reversed by passing an opposite current through the electrode interface during the off phase of the cycle. This may also require incorporation of active electronics on board to ensure a charge-balanced waveform. On the other hand, when the capacitive mechanism is employed, the interface capacitances can discharge during the off times through a simple resistance placed in parallel with the electrode contacts. The maximum value of this resistance can easily be calculated based on the value of the interface capacitance and the duty cycle of the stimulator. Some electrode materials that primarily use the capacitive mechanism are tantalum pentoxide (Ta_2Ox_5), titanium nitride (TiN),[72] and polymers like poly-3,4-ethylenedioxythiophene (PEDOT).[73] Tissue reaction to these materials and their long-term stability inside the hostile body environment as well as their mechanical durability are currently under investigation. [74,75]

VI. DESIGN OF AN IMPLANTATION TOOL

Implantation of a floating microstimulator demands a tool to hold the device during insertion, taking the place of the electrode substrate onto which the contacts are permanently attached in the case of traditional shank electrodes. With floating stimulators, however, the implantation tool is removed after insertion and the stab wound caused by the insertion tool will be repaired to a large extent by the immune system.[3] An additional advantage is that the surgeon can select the exact positions of the stimulators without being limited by the fixed interelectrode distances or needing to find a cortical or spinal area that will conform to the shape of the electrode substrate as in the case of multielectrode arrays. The implantation tool

should have current-delivering capabilities on its own in order to verify the implant location before deploying the microstimulator. Such a tool should be designed according to the physical dimensions of the microstimulator to minimize the tissue damage during insertion. A microfabricated silicon-based electrode carrier or a small-caliber stainless steel needle may function as an implantation tool.

VII. NEUROPROSTHETIC APPLICATIONS FOR FLOATING MICROSTIMULATORS

A mechanically floating microscale stimulator with no tethering wire attachments can solve the problems associated with movement of the electrodes *in situ.* In addition to the benefits discussed above, if individual microstimulators can be made smaller than a single shank of a multielectrode array, the volume of tissue replaced by each electrode is reduced. Also, because the microstimulators are discrete without any surface superstructure to connect them, there is no compression of the superficial neural tissue observed with multielectrode arrays. On the other hand, implantation of individual microstimulators may become prohibitively difficult with the increasing number of stimulation channels. With these trade-offs in mind, several neural prosthetic applications for floating microstimulators can be identified.

Intraspinal microstimulation can reportedly generate functionally useful motor activity with only a few channels of wired implants.[76,77] Chronically implantable microelectrode arrays for intraspinal stimulation currently do not have sufficient longevity to withstand high mobility of the spinal cord inside the vertebral column. Therefore, spinal cord applications would perhaps be the ones to benefit first from the availability of floating microstimulators. The drawing of Fig. 6 illustrates the concept of using an optical stimulator for intraspinal microstimulation. The idea can easily be extrapolated to acoustic and RF microstimulators. Potential applications include activation of intraspinal networks for coordinated movements of legs, as in locomotion,[78,79] upper extremities,[80] respiratory networks,[81] the bladder,[7,82] sexual function,[83] or the colon and anal sphincter.[84]

Another class of applications is to use the floating microstimulators for activation of cutaneous mechanoreceptors as a substitute for the lost sense of touch. A few of these devices can be implanted into the healthy skin, for instance around the upper arm, provided that they are small enough and each device can be activated selectively. This “smart tattoo” can then be used to substitute for the sense of touch in the hand that is impaired as a result of spinal cord injury. A similar approach can be visualized for the blind to provide them with an additional sensory modality on an area of the skin that is not normally used for probing the environment.

VIII. CONCLUSIONS

As the field of neuroprosthetics is growing rapidly, many applications demand implantable electrodes that can last a lifetime in the CNS and be minimally traumatic to the surrounding neural tissue. Wireless multielectrode arrays with built-in integrated microcircuits have been given much attention. Many applications dealing with stimulation of the sensory areas of the

cerebral cortex, such as visual and auditory prosthesis, require a large number of stimulation channels for their functionality. Thus, multielectrode arrays have been the focus of research to pave the way to clinical implementation of cortical neuroprosthetics. In contrast, a number of other neural prosthetic applications in the spinal cord can benefit from only a single or a few channels of stimulation. In addition, the spinal cord experiences much larger translational and rotational displacements than the brain, making the longevity of the electrodes and the tissue reaction the major challenges to overcome. In this review paper, submillimeter-size single-channel floating wireless stimulators are proposed as a possible approach to address these challenges. Wireless power coupling of passive microscale stimulating devices using infrared, RF, or acoustic methods has a potential to significantly improve the longevity and reduce the tissue trauma for mobile neural substrates such as the spinal cord. This article has discussed the design criteria for these three different potential means of wireless power transfer with a special emphasis on the optical method.

Acknowledgments

Special thanks to Douglas B. McCreery for commenting on the manuscript and Ammar Abdo for Monte Carlo simulations.

ABBREVIATIONS

CNS	central nervous system
RF	radio frequency
DC	direct current
PUS	pulsed ultrasound
PZT	lead zirconate titanate
NIR	near infrared
FLAME	floating light-activated micro-electrical
MEMS	micro-electromechanical
AF	activation function
CIC	charge injection capacity
PEDOT	poly-3,4- ethylenedioxythiophene

References

1. Hetke JF, Lund JL, Najafi K, Wise KD, Anderson DJ. Silicon ribbon cables for chronically implantable microelectrode arrays. IEEE Trans Biomed Eng. 1994 Apr; 41(4):314–21. [PubMed: 8063297]
2. McConnell GC, Rees HD, Levey AI, Gutekunst CA, Gross RE, Bellamkonda RV. Implanted neural electrodes cause chronic, local inflammation that is correlated with local neurodegeneration. J Neural Eng. 2009 Oct.6(5):056003. [PubMed: 19700815]

3. Biran R, Martin DC, Tresco PA. The brain tissue response to implanted silicon microelectrode arrays is increased when the device is tethered to the skull. J Biomed Mater Res A. 2007 Jul; 82(1): 169–78. [PubMed: 17266019]

4. Doessel O, Schlegel WC, Hassler C, Stieglitz T. Polymer-based approaches to improve the long term performance of intracortical neural interfaces. IFMBE Proceedings. 2009; 25(9):119–22.

5. McCreery D, Pikov V, Troyk PR. Neuronal loss due to prolonged controlled-current stimulation with chronically implanted microelectrodes in the cat cerebral cortex. J Neural Eng. 2010; 7(3): 036005. [PubMed: 20460692]

6. Liu X, McCreery DB, Bullara LA, Agnew WF. Evaluation of the stability of intracortical microelectrode arrays. IEEE Trans Neural Syst Rehabil Eng. 2006 Mar; 14(1):91–100. [PubMed: 16562636]

7. Pikov V, Bullara L, McCreery DB. Intraspinal stimulation for bladder voiding in cats before and after chronic spinal cord injury. J Neural Eng. 2007 Dec; 4(4):356–68. [PubMed: 18057503]

8. Ji S, Zhu Q, Dougherty L, Margulies SS. In vivo measurements of human brain displacement. Stapp Car Crash J. 2004 Nov.48:227–37. [PubMed: 17230268]

9. Zou H, Schmiedeler JP, Hardy WN. Separating brain motion into rigid body displacement and deformation under low-severity impacts. J Biomech. 2007; 40(6):1183–91. [PubMed: 16919640]

10. Conrad BP, Horodyski M, Wright J, Ruetz P, Rechtine GR 2nd. Log-rolling technique producing unacceptable motion during body position changes in patients with traumatic spinal cord injury. J Neurosurg Spine. 2007 Jun; 6(6):540–3. [PubMed: 17561742]

11. Borton DA, Song YK, Patterson WR, Bull CW, Park S, Laiwalla F, Donoghue JP, Nurmikko AV. Wireless, high-bandwidth recordings from non-human primate motor cortex using a scalable 16-Ch implantable microsystem. Conf Proc IEEE Eng Med Biol Soc. 2009; 2009:5531–4. [PubMed: 19964128]

12. Gregory JA, Borna A, Roy S, Wang X, Lewandowski B, Schmidt M, Najafi K. Low-cost wireless neural recording system and software. Conf Proc IEEE Eng Med Biol Soc. 2009; 2009:3833–6. [PubMed: 19965244]

13. Ghovanloo M, Najafi K. A wireless implantable multichannel microstimulating system-on-achip with modular architecture. IEEE Trans Neural Syst Rehabil Eng. 2007 Sep; 15(3):449– 57. [PubMed: 17894278]

14. Troyk PR, Rush AD. Inductive link design for miniature implants. Conf Proc IEEE Eng Med Biol Soc. 2009; 2009:204–9. [PubMed: 19964210]

15. Sahin M, Tie Y. Non-rectangular waveforms for neural stimulation with practical electrodes. J Neural Eng. 2007 Sep; 4(3):227–33. [PubMed: 17873425]

16. Wongsarnpigoon A, Grill WM. Genetic algorithm reveals energy-efficient waveforms for neural stimulation. Conf Proc IEEE Eng Med Biol Soc. 2009; 2009:634–7. [PubMed: 19964233]

17. Poon ASY, O'Driscoll S, Meng TH. Optimal frequency for wireless power transmission into dispersive tissue. IEEE Trans Anten Propag. 2010; 58(5):1739–50.

18. Heetderks WJ. RF powering of millimeter- and submillimeter-sized neural prosthetic implants. IEEE Trans Biomed Eng. 1988; 35(5):323–7. [PubMed: 3397079]

19. Loeb GE, Peck RA, Moore WH, Hood K. BION system for distributed neural prosthetic interfaces. Med Eng Phys. 2001 Jan; 23(1):9–18. [PubMed: 11344003]

20. Furse, C.; Christensen, DA.; Durney, CH. Basic Introduction to Bioelectromagnetics. 2. CRC Press; 2009.

21. Schepps JL, Foster KR. The UHF and microwave dielectric properties of normal and tumour tissues: variation in dielectric properties with tissue water content. Phys Med Biol. 1980; 25(6): 1149. [PubMed: 7208627]

22. Augustine, R. Doctoral Thesis: Electromagnetic modelling of human tissues and its application on the interaction between antenna and human body in the BAN context. Paris: Université Paris-Est; 2009. http://tel.archivesouvertes.fr/tel-00499255

23. Zhadobov M, Sauleau R, Le Drean Y, Alekseev SI, Ziskin MC. Numerical and experimental millimeter-wave dosimetry for in vitro experiments. IEEE Trans Microwave Theory Tech. 2008; 56(12):2998–3007.

24. Loeb GE, Richmond FJ, Baker LL. The BION devices: injectable interfaces with peripheral nerves and muscles. Neurosurg Focus. 2006; 20(5):E2. [PubMed: 16711659]
25. Lee U, Song KD, Park Y, Varadan VK, Choi SH. Perspective in nanoneural electronic implants with wireless power-feed and sensory control. J Nanotechnol Eng Med. 2010; 1(2):021007.
26. Sang HC, Song KD, Golembiewskii W, Chu S-H, King GC. Microwave power for smart material actuators. Smart Mater Struct. 2004; 13(1):38–48.
27. van Schuylenbergh, K.; Puers, R. Inductive Powering: Basic Theory and Application to Biomedical Systems. Springer; 2009.
28. Ibrahim T, Abraham D, Rennaker R. Electromagnetic power absorption and temperature changes due to brain machine interface operation. Annals Biomed Eng. 2007; 35(5):825–34.
29. Foster KR. Electromagnetic field effects and mechanisms. IEEE Eng Med Biol Mag. 1996; 15(4): 50–6.
30. Thornton TJ. Physics and applications of the Schottky junction transistor. IEEE Trans Electron Devices. 2001 Oct; 48(10):2421–7.
31. Schulman JH. The feasible FES system: Battery powered BION stimulator. Proc IEEE. 2008 Jul; 96(7):1226–39.
32. Whitehurst TK, Schulman JH, Jaax KN, Carbunaru R. The Bion® microstimulator and its clinical applications. Implantable Neural Prostheses 1. 2009:253–73.
33. Ziaie B, Nardin MD, Coghlan AR, Najafi K. A single-channel implantable microstimulator for functional neuromuscular stimulation. IEEE Trans Biomed Eng. 1997 Oct; 44(10):909–20. [PubMed: 9311160]
34. Zealear DL, Swelstad MR, Sant'Anna GD, Bannister RA, Billante CR, Rodriguez RJ, Garren KC, Billante MJ, Champney MS. Determination of the optimal conditions for laryngeal pacing with the Itrel II implantable stimulator. Otolaryngol Head Neck Surg. 2001 Sep; 125(3):183–92. [PubMed: 11555752]
35. Echt DS, Cowan MW, Riley RE, Brisken AF. Feasibility and safety of a novel technology for pacing without leads. Heart Rhythm. 2006; 3(10):1202–6. [PubMed: 17018352]
36. Lee KL, Tse H-F, Echt DS, Lau C-P. Temporary lead-less pacing in heart failure patients with ultrasound- mediated stimulation energy and effects on the acoustic window. Heart Rhythm. 2009; 6(6):742–8. [PubMed: 19427274]
37. Phillips, WB.; Tow, BC.; Larson, PJ., editors. IEEE/EMBS. 2003. An Ultrasonically- Driven Piezoelectric Neural Stimulator.
38. Zhu Y, Moheimani SOR, Yuce MR. Ultrasonic energy transmission and conversion using a 2-D MEMS resonator. IEEE Electron Dev Lett. 2010; 31(4):374–6.
39. Vykhodtseva NI, Hynynen K, Damianou C. Pulse duration and peak intensity during focused ultrasound surgery: theoretical and experimental effects in rabbit brain in vivo. Ultrasound Med Biol. 1994; 20(9):987–1000. [PubMed: 7886858]
40. FDA. Information for manufacturers seeking marketing clearance of diagnostic ultrasound systems and transducers. Rockville, MD: Center for Devices and Radiological Health; 1997.
41. Choi JJ, Pernot M, Brown TR, Small SA, Konofagou EE. Spatio-temporal analysis of molecular delivery through the blood-brain barrier using focused ultrasound. Physics Med Biol. 2007; 52(18):5509.
42. Tyler WJ, Tufail Y, Finsterwald M, Tauchmann ML, Olson EJ, Majestic C. Remote excitation of neuronal circuits using low-intensity, low-frequency ultrasound. PLoS One. 2008; 3(10):e3511. [PubMed: 18958151]
43. Benditt DG, Goldstein M, Belalcazar A. The leadless ultrasonic pacemaker: A sound idea? Heart Rhythm. 2009; 6(6):749–51. [PubMed: 19467502]
44. Goto K, Nakagawa T, Nakamura O, Kawata S. Near-infrared light transcutaneous telemetry system having an implantable transmitter driven by external laser irradiation. Rev Sci Instrum. 2001; 72(7):3079–85.
45. Goto K, Nakagawa T, Nakamura O, Kawata S. Transcutaneous photocoupler for transmission of biological signals. Opt Lett. 2002; 27(20):1797–9. [PubMed: 18033367]

46. Loudin JD, Simanovskii DM, Vijayraghavan K, Sramek CK, Butterwick AF, Huie P, McLean GY, Palanker DV. Optoelectronic retinal prosthesis: system design and performance. J Neural Eng. 2007; 4(1):S72–S84. [PubMed: 17325419]
47. Schubert MB, Hierzenberger A, Lehner HJ, Werner JH. Optimizing photodiode arrays for the use as retinal implants. Sensor Actuat A Phys. 1999; 74(1–3):193–7.
48. Song Y-K, Patterson WR, Bull CW, Beals J, Hwang N, Deangelis AP, Lay C, McKay JL, Nurmikko AV, Fellows MR, Simeral JD, Donoghue JP, Connors BW. Development of a chip-scale integrated microelectrode/microelectronic device for brain implantable neuroengineering applications. IEEE Trans Neural Syst Rehabil Eng. 2005; 13(16003903):220–6. [PubMed: 16003903]
49. Zomorrodian A, Wu NJ, Song Y, Stahl S, Ignatiev A, Trexler EB, Brady, Garcia C. Micro Photo detector fabricated of ferroelectric-metal hetero-structure. Jpn J Appl Phys. 2005; 44:6105–8.
50. Pintilie L, Vrejoiu I, Le Rhun G, Alexe M. Short-circuit photocurrent in epitaxial lead zirconate-titanate thin films. J Appl Phys. 2007; 101(6):064109–8.
51. Choi T, Lee S, Choi YJ, Kiryukhin V, Cheong S-W. Switchable ferroelectric diode and photovoltaic effect in BiFeO3. Science. 2009 Apr 3; 324(5923):63–6. [PubMed: 19228998]
52. Aravanis AM, Wang LP, Zhang F, Meltzer LA, Mogri MZ, Schneider MB, Deisseroth K. An optical neural interface: in vivo control of rodent motor cortex with integrated fiberoptic and optogenetic technology. J Neural Eng. 2007; 4(3):S143. [PubMed: 17873414]
53. McDonagh C, Burke CS, MacCraith BD. Optical chemical sensors. Chem Reviews. 2008; 108(2): 400–22.
54. Tokuda T, Hiyama K, Sawamura S, Sasagawa K, Terasawa Y, Nishida K, Kitaguchi Y, Fujikado T, Tano Y, Ohta J. CMOS-based multichip networked flexible retinal stimulator designed for image-based retinal prosthesis. IEEE Trans Electron Devices. 2009; 56(11):2577–85.
55. Piyathaisere DV, Margalit E, Chen SJ, Shyu JS, D'Anna SA, Weiland JD, Grebe RR, Grebe L, Fujii G, Kim SY, Greenberg RJ, De Juan E Jr, Humayun MS. Heat effects on the retina. Ophthalmic Surg Lasers Imaging. 2003 Mar-Apr;34(2):114–20. [PubMed: 12665226]
56. Ackermann DM, Smith B, Xiao-Feng W, Kilgore KL, Hunter Peckham P. Designing the optical interface of a transcutaneous optical telemetry link. IEEE Trans Biomed Eng. 2008; 55(4):1365–73. [PubMed: 18390327]
57. Laser Institute of America. American National Standard for Safe Use of Lasers, ANSI Z136.1–2000. Laser Institute of America; 2007.
58. Rahman S, Sahin M. Finite element analysis of a microelectrode on a substrate. Conf Proc IEEE Eng Med Biol Soc. 2004; 6:4157–9. [PubMed: 17271217]
59. Gray, KM.; Innamuri, HK.; Tayebi, A.; Sahin, M., editors. IEEE/EMBS. 2003. Voltage field generated by a single photodiode in a volume conductor: Simulation and measurements.
60. Abdo A, Sahin A. Feasibility of neural stimulation with floating light activated micro-electrical stimulators. Tran Biomed Circuits and Systems. 2010 (in press).
61. Eggert HR, Blazek V. Optical properties of human brain tissue, meninges, and brain tumors in the spectral range of 200 to 900 nm. Neurosurgery. 1987 Oct; 21(4):459–64. [PubMed: 3683777]
62. Sharma HS, Hoopes PJ. Hyperthermia induced pathophysiology of the central nervous system. Int J Hyperthermia. 2003 May-Jun;19(3):325–54. [PubMed: 12745974]
63. Zimmermann, H. Integrated Silicon Optelectronics. New York: Springer; 2000.
64. Cho Y, Ivanisevic A. In vitro assessment of the biocompatibility of chemically modifed GaAs surfaces. Nanobiotechnology. 2006; 2:51–9.
65. Feili D, Schuettler M, Doerge T, Kammer S, Stieglitz T. Encapsulation of organic field effect transistors for flexible biomedical microimplants. Sensors Actuat A Phys. 2005; 120:9.
66. Pikov V. Clinical applications of intraspinal microstimulation. Proc IEEE. 2008; 96(7):1120–8.
67. Chao X, Jun S, Bin Z, Guangming W, Xiang X. Study on parylene/SiO2 composite films for protection of KDP crystals. J Sol-Gel Sci Technol. 2008; 45:319–24.
68. Nunez, PL.; Srinivasan, R. Electric Fields of the Brain: The Neurophysics of EEG. Oxford Univesity Press; 2006. Current sources in a homogeneous and isotropic medium.

69. Rattay F. Analysis of models for external stimulation of axons. IEEE Trans Biomed Eng. 1986 Oct; 33(10):974–7. [PubMed: 3770787]

70. Cogan SF, Troyk PR, Ehrlich J, Plante TD, Detlefsen DE. Potential-biased, asymmetric waveforms for charge-injection with activated iridium oxide (AIROF) neural stimulation electrodes. IEEE Trans Biomed Eng. 2006 Feb; 53(2):327– 32. [PubMed: 16485762]

71. Cogan SF. In vivo and in vitro differences in the charge-injection and electrochemical properties of iridium oxide electrodes. Conf Proc IEEE Eng Med Biol Soc. 2006; 1:882–5. [PubMed: 17946868]

72. Zhou, DM.; Greenberg, RJ., editors. IEEE/EMBS. 2003. Electrochemical characterization of titanium nitride microelectrode arrays for charge-injection applications.

73. Ludwig KA, Uram JD, Yang J, Martin DC, Kipke DR. Chronic neural recordings using silicon microelectrode arrays electrochemically deposited with a poly(3,4-ethylenedioxythiophene) (PEDOT) film. J Neural Eng. 2006 Mar; 3(1):59–70. [PubMed: 16510943]

74. Cui XT, Zhou DD. Poly (3,4-ethylenedioxythiophene) for chronic neural stimulation. IEEE Trans Neural Syst Rehabil Eng. 2007 Dec; 15(4):502–8. [PubMed: 18198707]

75. Han M, McCreery DB. A new chronic neural probe with electroplated iridium oxide microelectrodes. Conf Proc IEEE Eng Med Biol Soc. 2008; 2008:4220–1. [PubMed: 19163643]

76. Saigal R, Renzi C, Mushahwar VK. Intraspinal microstimulation generates functional movements after spinal-cord injury. IEEE Trans Neural Syst Rehabil Eng. 2004 Dec; 12(4):430–40. [PubMed: 15614999]

77. Mushahwar VK, Gillard DM, Gauthier MJA, Prochazka A. Intraspinal microstimulation generates locomotor-like and feedback-controlled movements. IEEE Trans Neural Syst Rehabil Eng. 2002; 10:68–81. [PubMed: 12173741]

78. McCreery D, Pikov V, Lossinsky A, Bullara L, Agnew W. Arrays for chronic functional microstimulation of the lumbosacral spinal cord. IEEE Trans Neural Syst Rehabil Eng. 2004 Jun; 12(2):195–207. [PubMed: 15218934]

79. Tai C, Booth AM, Robinson CJ, de Groat WC, Roppolo JR. Multi-joint movement of the cat hindlimb evoked by microstimulation of the lumbosacral spinal cord. Exp Neurol. 2003 Oct; 183(2):620–7. [PubMed: 14552903]

80. Moritz CT, Lucas TH, Perlmutter SI, Fetz EE. Forelimb movements and muscle responses evoked by microstimulation of cervical spinal cord in sedated monkeys. J Neurophysiol. 2007 Jan; 97(1): 110–20. [PubMed: 16971685]

81. Alilain WJ, Li X, Horn KP, Dhingra R, Dick TE, Herlitze S, Silver J. Light-induced rescue of breathing after spinal cord injury. J Neurosci. 2008 Nov 12; 28(46):11862–70. [PubMed: 19005051]

82. Grill WM, Bhadra N, Wang B. Bladder and urethral pressures evoked by microstimulation of the sacral spinal cord in cats. Brain Res. 1999 Jul 31; 836(1–2):19–30. [PubMed: 10415401]

83. Tai C, Booth AM, de Groat WC, Roppolo JR. Penile erection produced by microstimulation of the sacral spinal cord of the cat. IEEE Trans Rehabil Eng. 1998 Dec; 6(4):374–81. [PubMed: 9865884]

84. Tai C, Booth AM, de Groat WC, Roppolo JR. Colon and anal sphincter contractions evoked by microstimulation of the sacral spinal cord in cats. Brain Res. 2001 Jan 19; 889(1–2):38–48. [PubMed: 11166684]

85. Johns M, Giller C, German D, Liu H. Determination of reduced scattering coefficient of biological tissue from a needle-like probe. Opt Express. 2005 Jun 27; 13(13):4828–42. [PubMed: 19498468]

86. Gebhart SC, Lin WC, Mahadevan-Jansen A. In vitro determination of normal and neoplastic human brain tissue optical properties using inverse adding-doubling. Physics in Medicine and Biology. 2006; 51:2011–27. [PubMed: 16585842]

87. Ibrahim TS, Abraham D, Rennaker RL. Electromagnetic power absorption and temperature changes due to brain machine interface operation. Ann Biomed Eng. 2007 May.35(5):825. [PubMed: 17334681]

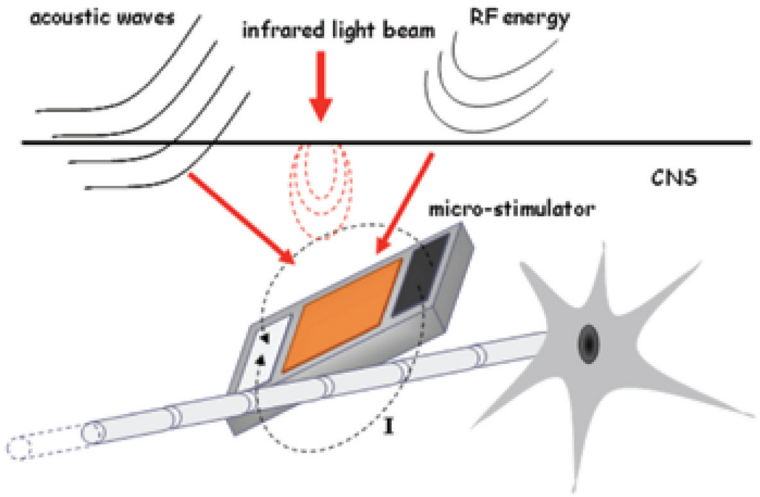

FIGURE 1.

A generic passive floating microstimulator implanted in the CNS. Stimulus energy is transferred to the device through acoustic, optic, or RF telemetry. Energy is converted to electric current and injected into the medium via the bipolar contacts to activate the nearby neural structures. The stimulus parameters are controlled by the external energy source on a pulse-by-pulse basis. The external energy source may be located just outside the dura matter or as an extracorporeal device depending on the efficiency of coupling.

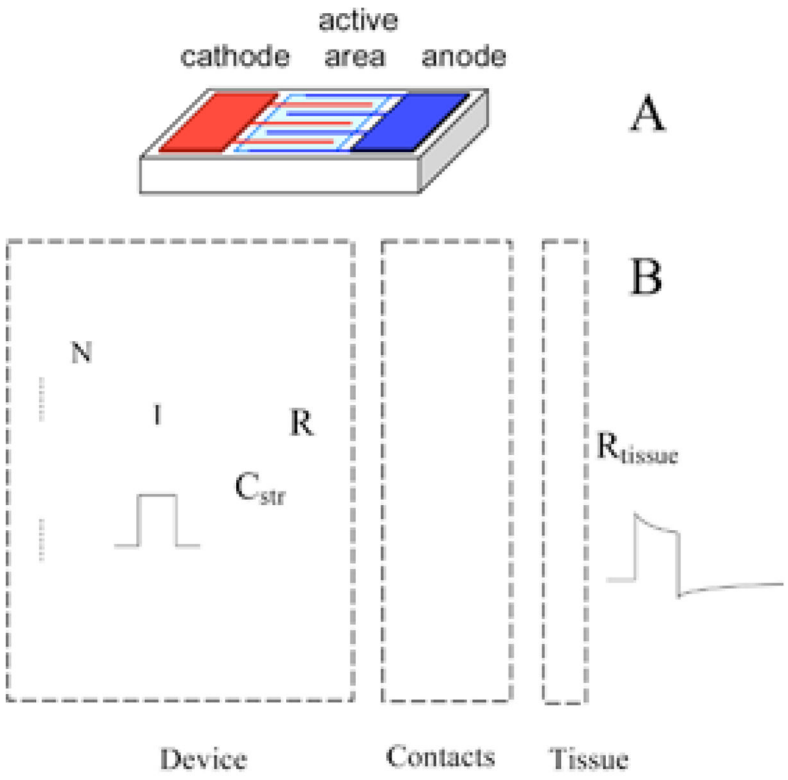

FIGURE 2.

Electrical model of the FLAME stimulators, [60] which includes multiple photodiodes in series to increase the output voltage compliance, the interface with the tissue at the contacts, and the tissue impedance (B). The drawing on top shows the arrangement of the photodiode active area and the contacts on the wafer (A). Some decrease of output current occurs during the pulse due to the current that flows through the intrinsic diodes as the device voltage is increasing with charging of contact capacitors. Contact capacitors are discharged passively through the parallel resistor (R) during the off phase of the pulse cycle. A small stray capacitor (C_{str}) is placed between the device terminals during fabrication.

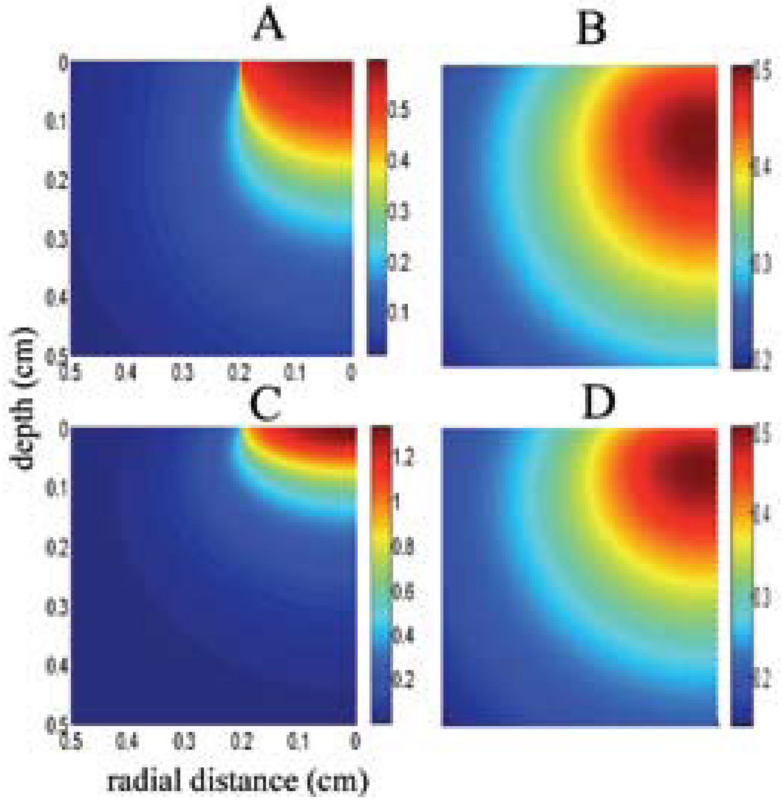

FIGURE 3.

Simulated NIR photon density (W/cm^3) inside the human gray (A) and white (B) matters due to a 0.2 cm radius NIR beam and the resulting temperature elevations in the tissue (C for gray and D for white). The NIR light beam is aimed from the top to the center of the cylindrical volume with a radius of 0.5 cm. Because of cylindrical symmetry, plots are made only for one half of the vertical cross sectional area. Note that maximum temperature is observed not at the surface but at 1.2 mm and 0.7 mm below the surface, respectively. Absorption and scattering coefficients for human gray and white matters were adopted from Refs. 85 and 86 and thermal conductivity of gray (0.57) and white (0.5 Wm^{-1}°C^{-1}) matters from Ref. 87.

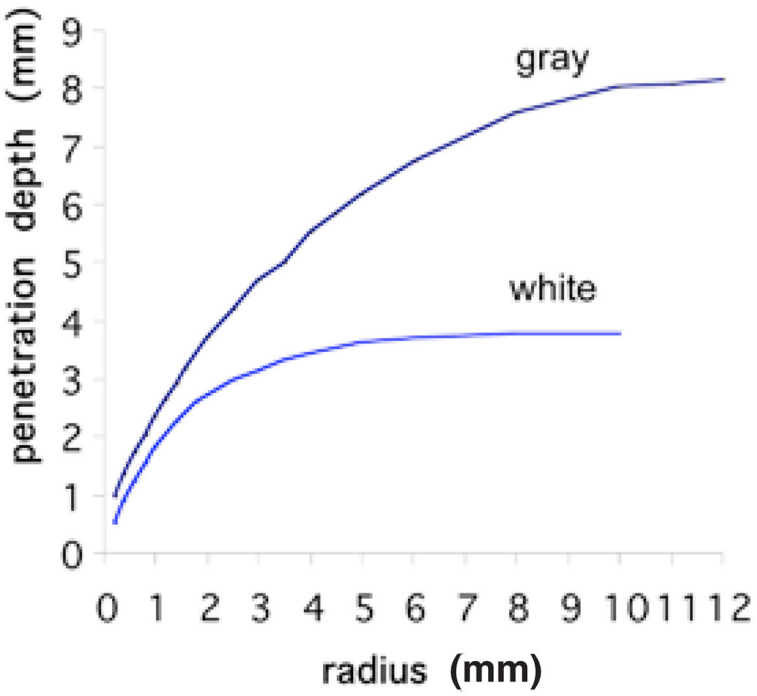

FIGURE 4.

Simulated depth of penetration (defined as the depth where incident light intensity is reduced to 37%) for NIR light into human gray and white matters as a function of beam radius. A flat profile circular beam is simulated using a Monte Carlo model (http://labs.seas.wustl.edu/bme/Wang/mc.html). Penetration depth increases with beam radius while the photon density (W/cm^2) is kept constant at the surface. Plots suggest that NIR penetrates twice as readily into the gray matter. The plots plateau at a depth of about 4 mm of beam radius for the white matter and 10 mm for the gray matter.

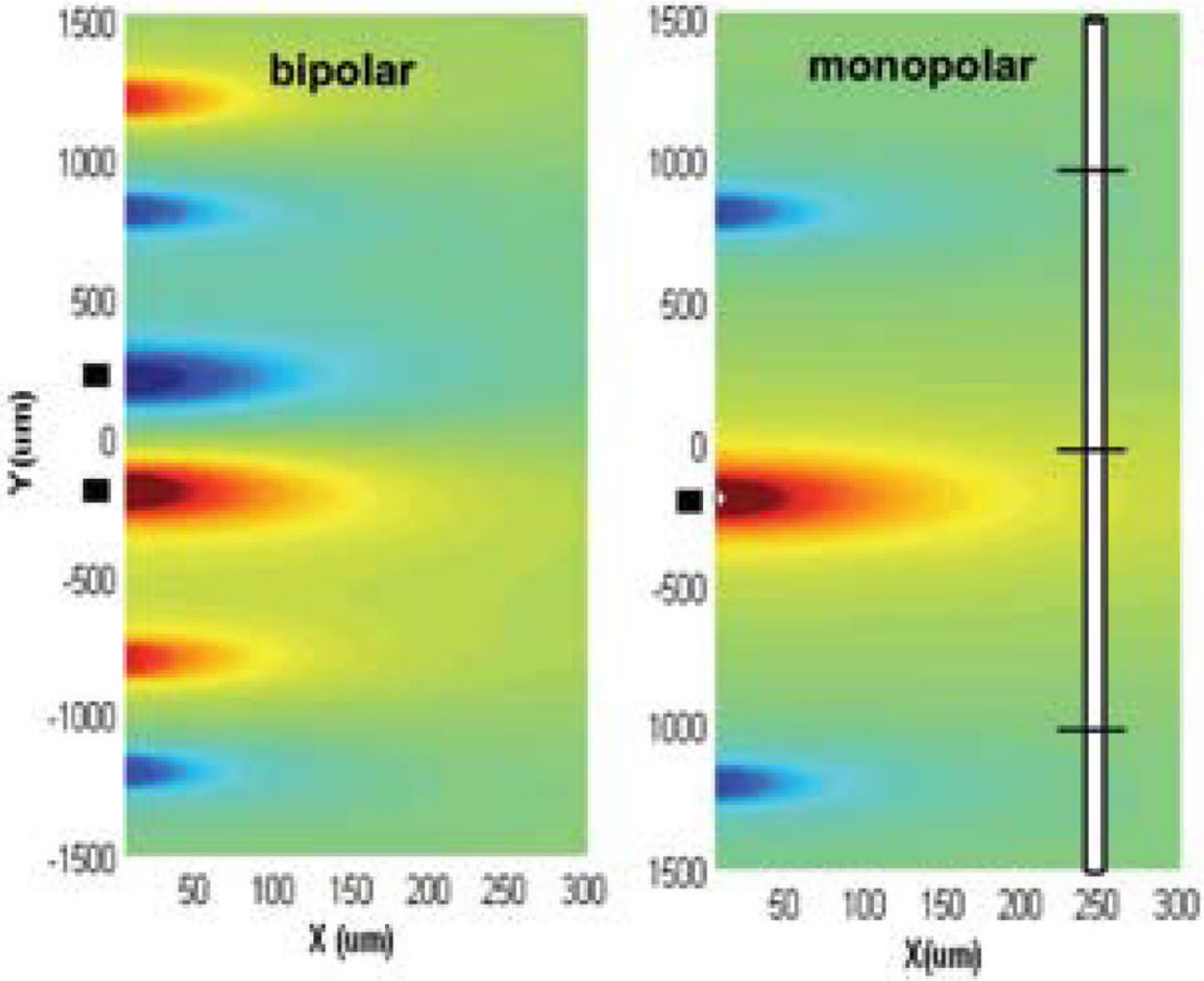

FIGURE 5.

Comparison of activation function generated by bipolar (left plot) and monopolar (right plot) electrodes for a 10-μm myelinated axon placed vertically on the page. AF is calculated as the second derivative of the extracellular voltage along the axon.[69] The vertical positioning of the axon and its three central nodes are shown on the right for Y = 0, X = 250 μm. The X,Y coordinates in the AF plots indicate the position of the central node as the fiber is moved around. The activation function changes as indicated by the color (red positive, blue negative) as a function of vertical and horizontal displacements of the axon with respect to the electrodes. Contact locations are indicated with black blocks on the left of each plot. Center-to-center separation between the anode and cathode is 400 μm for the bipolar electrodes. The monopolar cathodic electrode is located at X = 0, Y = −200 μm. The side lobes of the activation function on each side of the electrodes occur where the off-center nodes of Ranvier line up with the contact locations.

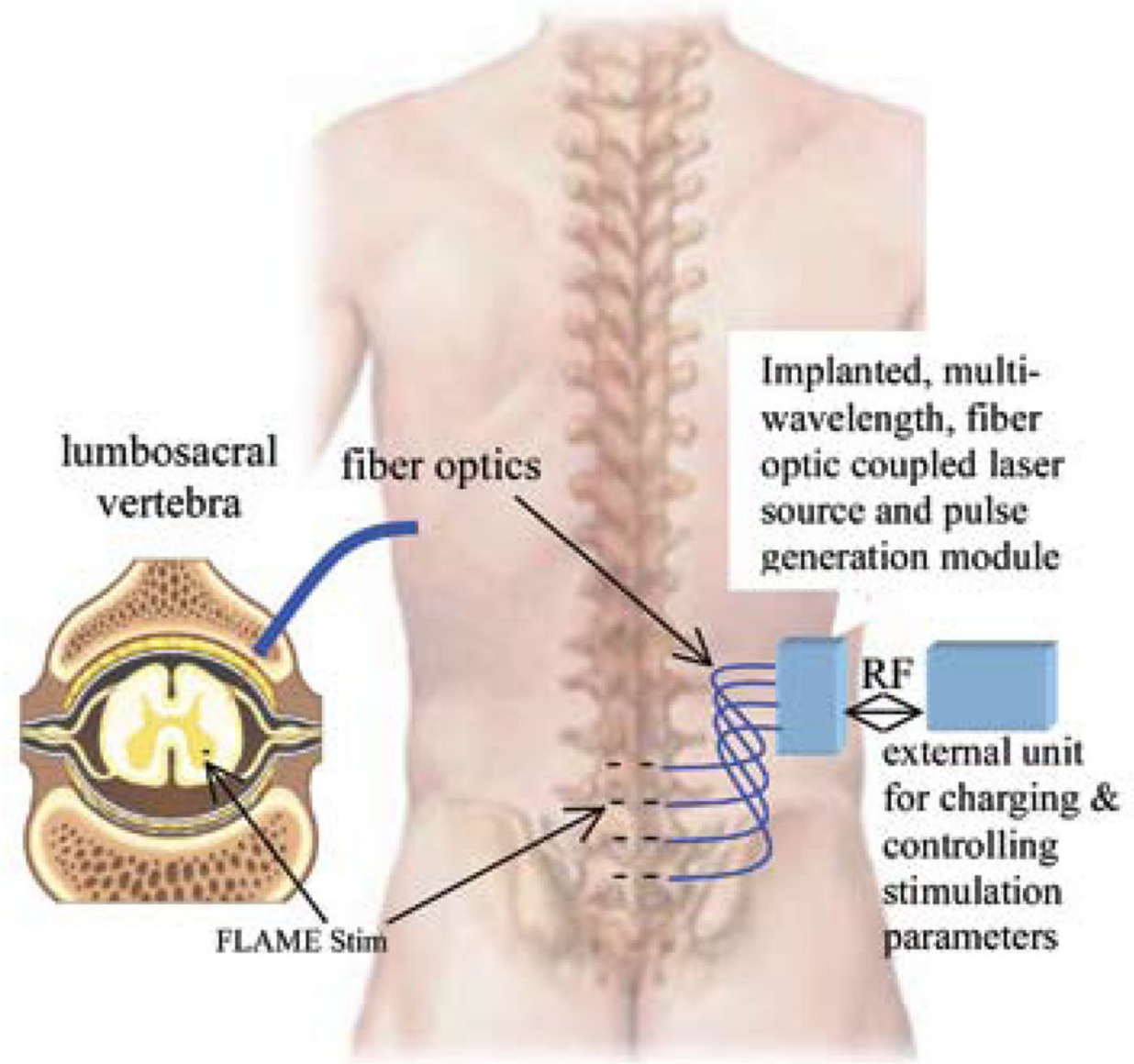

FIGURE 6.

Microstimulation of the lumbosacral spinal cord using an optical, floating microstimulator is envisioned as shown. The internal unit will activate multiple microstimulators at different wavelengths through optical fibers.